Atmos. Chem. Phys. Discuss., https://doi.org/10.5194/acp-2017-1157
Manuscript under review for journal Atmos. Chem. Phys.
Discussion started: 12 December 2017

Atmospheric Chemistry and Physics Discussions

Symptoms of total ozone recovery inside the Antarctic vortex during Austral spring

Andrea Pazmino[1], Sophie Godin-Beekmann[1], Alain Hauchecorne[1], Chantal Claud[2], Sergey Khaykin[1], Florence Goutail[1], Elian Wolfram[3], Jacobo Salvador[3,4,5], Eduardo Quel[3]

[1]LATMOS, UVSQ Univ. Paris Saclay, UPMC Univ. Paris 06, CNRS, Guyancourt, France
[2]LMD, CNRS, Ecole Polytechnique, Palaiseau, France
[3]CEILAP-UNIDEF (MINDEF-CONICET), UMI-IFAECI-CNRS-3351, Villa Martelli, Argentina
[4]Universidad Tecnológica Nacional, Facultad Regional Bs. As. (UTN-FRBA), Ciudad Autónoma de Bs. As., Argentina
[5]Universidad Nacional de la Patagonia Austral, Unidad Académica Río Gallegos (UNPA-UARG) and CIT-CONICET Río Gallegos, Argentina

Correspondence to: Andrea Pazmino (andrea.pazmino@latmos.ipsl.fr)

Abstract. The long-term evolution of total ozone column inside the Antarctic polar vortex is investigated over the 1980-2016 period. Trend analyses are performed using a multilinear regression (MLR) model based on various proxies (heat flux, Quasi-Biennial Oscillation, solar flux, Antarctic Oscillation and aerosols). Annual total ozone column corresponding to the mean monthly values inside the vortex in September and during the period of maximum ozone depletion from September 15th to October 15th are used. Total ozone columns from combined SBUV, TOMS and OMI satellite datasets and the Multi-Sensor Reanalysis (MSR-2) dataset are considered in the study. Ozone trends are computed by a piecewise trend model (PWT) before and after the turnaround in 2001. In order to evaluate total ozone within the vortex, two classification methods are used, based on the potential vorticity gradient as a function of equivalent latitude. The first standard one considers this gradient at a single isentropic level (475K or 550K), while the second one uses a range of isentropic levels between 400K and 600K. The regression model includes a new proxy that represents the stability of the vortex during the studied month period. The determination coefficient (R^2) between observations and modeled values increases by ~0.05 when this proxy is included in the MLR model. The higher R^2 (0.93-0.95) and the minimum residuals are observed for the second classification method for both datasets and months periods.

Trends in September are statistically significant at 2 sigma level over 2001-2016 period with values ranging between 1.85 and 2.67 DU yr^{-1} depending on the methods and data sets. This result confirms the recent studies of Antarctic ozone healing during that month. Trends after 2001 are 2 to 3 times lower than before the turnaround year as expected from the response to the slowly ozone-depleting substances decrease in Polar regions.

Estimated trends in the 15Sept-15Oct period are smaller than in September. They vary from 1.15 to 1.78 DU yr^{-1} and are hardly significant at 2σ level.

Ozone recovery is also confirmed by a steady decrease of the relative area of total ozone values lower than 150 DU within the vortex in the 15Sept-15Oct period since 2010. Comparison of the evolution of the ozone hole area in September and October shows a decrease in September, confirming the later formation of the ozone hole during that month.

1 Introduction

The evolution of total ozone content (TOC) in Antarctica during Austral spring is deeply linked to the important stratospheric ozone decline that was highlighted for the first time by Chubachi et al., 1984 and Farman et al., 1985. Nowadays the photochemical and microphysical processes leading to the massive and seasonal destruction of ozone in Polar Regions are well understood. The latest Ozone Assessment Reports (WMO, 2007, 2011, 2014) have confirmed the stabilization of ozone loss in Antarctica since 2000. The challenge now is to assess the impact of the observed reduction in the concentration of ozone depleting substances (evaluated in the polar regions to ~10% in 2013 from the peak values in

2000, WMO, 2014) on the amplitude of the ozone destruction every year. During the last decade, several studies have been carried out to quantify a possible increase in total ozone column in the Antarctic polar vortex in spring directly linked to this decrease in the polar stratosphere. Most analyses use multi-parameter regression models with different proxies to represent the interannual variability of ozone as the 11 year solar cycle, the quasi-biennial oscillation (QBO), volcanic aerosols or eddy heat flux (Salby et al., 2012; Kuttipurath et al., 2013; De Laat et al., 2015). These studies generally show a significant increase of TOC since 2000 for September-November average period but they differ on the proxies used for the quantification of ozone inter-annual variability. De Laat et al. (2015) used a "big data" ensemble approach to calculate trends. Several scenarios were considered for the period of ozone data-set and for the different proxy records. They found that significance of trend could vary from negligible to 100% significant depending on the scenario considered. They have also determined the optimal proxy records and ozone record scenarios.

Solomon et al. (2016) evaluated ozone trend using a Specified Dynamics version of Whole Atmosphere Community Climate Model (SD-WACCM). The authors have shown a significant healing in September but not in October where ozone content is deepest during the first two weeks. They also explain the difficulty of estimating trend in October by the large variability of ozone linked to temperature variations and transport. The baroclinicity of the polar vortex in October and its displacement in relation to the geographic pole can explain the variability of the total ozone series averaged during the month of October.

The direct link between the positive trend and the reduction of ozone-depleting substances (ODS) remains thus an open question, given the natural variability of the Antarctic vortex and the possible contribution of greenhouse gases (GHGs) to the trend (Chipperfield et al., 2017).

The purpose of the present paper is to provide an update of ozone evolution inside the Antarctic vortex during the last decades taking into account the vortex baroclinicity. The main aim is to determine the different contributions to ozone inter-annual variability and to estimate the post 2001 total ozone trend and related significance for different periods: September, which corresponds to the full development of Polar ozone depletion and mid-September to mid-October when the maximum ozone loss is reached.

This study is organized as follows. Ozone dataset from satellites and multi-sensor reanalysis are presented in Sect. 2 and the description of the method used for total ozone column classifications inside the vortex in Sect. 3. Influence of vortex baroclinicity on total ozone column inside the vortex is assessed in Sect. 4 using a new classification method and standard one at a single isentropic level. Ozone trends before and after a turnaround year calculated for September and mid-September to mid-October are presented and discussed in Sect. 5. The temporal evolution of the number of very low total ozone values inside the vortex is evaluated in Section 6. Conclusions are finally presented in Sect. 7.

2 Total ozone column data series

Total ozone global fields from satellite observations (TOMS, OMI and SBUV) and multi-sensor reanalysis (MSR) are used in this study to cross-check trend estimation before and after a turnaround year over the 1980-2016 period.

2.1 Space-borne observations

Total ozone columns data series of NASA's Total Ozone Mapping Spectrometer (TOMS) instrument onboard Nimbus-7 (N7) and Earth Probe (EP) between 1980 and 2004 are used. The instrument is a single monochromator that was designed for near-nadir measurements of the total ozone column (e.g. McPeters et al., 1998). TOMS measures the backscattering of solar radiation by the Earth's atmosphere in six 1nm-bands of ultraviolet wavelength between 306 nm to 380 nm, more or less absorbed by ozone. Total ozone column is inferred from the ratio of two wavelengths, 317.5 nm strongly absorbed by ozone and 331.2 nm weakly absorbed (Bhartia and Wellemeyer, 2002). Level 3 gridded TV8 data of 1.0° (lat) x 1.25° (lon) of total ozone columns of TOMS were used in this work and are available from the Goddard Earth Sciences Distributed

Information and Services Center (GES DISC) in simple ASCII format in the NASA anonymous ftp site (ftp://toms.gsfc.nasa.gov/pub/*satellite*/data/ozone/)

Ozone total column observations of Ozone Monitoring Instrument (OMI) onboard Aura satellite are also used to continue TOMS measurements from 2005 to 2016. The OMI instrument is a nadir viewing hyperspectral imaging in a push-broom mode. OMI measures the solar backscatter radiation in the complete spectrum of the ultraviolet/visible wavelength range (270 nm - 500 nm) with 0.5 nm spectral resolution (Levelt et al., 2006). Total ozone column used in this work was retrieved using TV8 algorithm, hereafter referred to as OMIT in order to maintain continuity with TOMS data record (McPeters et al., 2008). Level 3 daily gridded data of OMIT with better spatial resolution (1.0° x 1.0°) than TOMS is used. Data are also available on NASA anonymous ftp site.

The total ozone column data series was combined by using specific satellite data over the following periods: TOMS-N7 (1980-1992), TOMS-EP (1996-2004) and OMIT (2005-2016). Note that data of 1993-1995 are sparse or missing for the September-October period. In order to complete the data series, total ozone column observations of Solar Backscatter Ultraviolet Radiometer (SBUV) onboard NOAA-9 (SBUV-N9) were used for those years. SBUV is a nadir viewing double grating monochromator instrument that measures backscattering of solar radiation by the Earth's atmosphere at 12 wavelengths from 250 nm to 340 nm (Frederick et al., 1986). Daily files of individual measurements (level 2) of version 8.6 (V8.6) are used in this work and are available on NASA anonymous ftp site (ftp://toms.gsfc.nasa.gov/pub/sbuv/NOAA09/). An overview of the V8.6 SBUV data record is presented in McPeters et al., 2013.

TOMS/OMIT and SBUV data series have previously been used in different scientific studies of ozone recovery in the Southern polar region (Salby et al., 2012; Kuttipurath et al. 2013; Solomon et al., 2016, Weber et al., 2017). The bias induced by using SBUV data on 1993-1995 is discussed in Sect. 4. Hereafter the 1980-2016 composite satellite total ozone series will be called SAT.

2.2 Multi-Sensor reanalysis

Ozone Multi-Sensor Reanalysis version 2 (MSR-2) provides global assimilated ozone fields for the period 1980-2015 based on 14 satellite data sets (van der A et al., 2015). Ozone data of 2016 were not yet available at the time of writing this paper and are therefore not included in the study. The 14 polar orbiting satellites measuring in the near-ultraviolet Huggins band were corrected to construct a merged satellite data series that are assimilated within the chemistry-transport assimilation model TM3-DAM to obtain MRS-2 data (see van der A et al., 2010 for a detailed description and van der A et al., 2015 for last improvements of the assimilation model). Corrections of offset, trends and variations of solar zenith angle and temperature in stratosphere were computed in satellite data sets by comparisons with individual ground-based Dobson and Brewer measurements from World Ozone and Ultraviolet Data Center (WOUDC). Those corrections are specified in van der A et al. (2015), table 2.

Daily gridded forecast ozone data of MSR-2 at 12 UTC and spatial resolution of 0.5° x 0.5° were used in this work and they are available from the Tropospheric Emission Monitoring Internet Service (TEMIS) of KNMI/ESA (http://www.temis.nl/protocols/o3field/data/msr2/).

Different studies on trends in the South Hemisphere have used MRS-2 data (Kuttipurath et al., 2013, de Laat et al., 2015). Hereafter the 1980-2015 ozone series will be called MSR-2.

3 Data classification within the vortex

In order to consider total ozone columns only within the polar vortex, the data classification is performed by evaluating the vortex's position at different isentropic levels from May 1st to December 31, each year. Two classification methods are then applied in order to evaluate the impact of baroclinicity of the vortex on the averaged total ozone columns in both studied

depletion periods. The first one is based on a single isentropic level, while the second one considers a range of isentropic levels.

3.1 Vortex position

For each day of the studied periods, the vortex position is determined by using a 2-D quasi-conservative coordinate system (equivalent latitude/potential temperature) described by McIntyre and Palmer (1984) where the pole in equivalent latitude (EL) corresponds to the position of maximum potential vorticity (PV). This conservative system is computed from PV field simulated by the Modélisation Isentrope du transport Mésoéchelle de l'Ozone Stratosphérique par Advection (MIMOSA) PV advection model (Hauchecorne et al., 2002). The model was forced by ERA-Interim (Dee et al., 2011) meteorological data (2.5°x 2.5°) of European Centre for Medium-Range Weather Forecasts (ECMWF). Daily advected PV fields (1°×1°) on the 30°S–90°S latitude band at 12 UTC are used to calculate EL on the isentropic level range between 400K and 600K with a step of 25K.

Following Nash et al. (1996), PV is evaluated as a function of EL and three particular regions are identified: inside the vortex, characterized by high PV values, at the vortex edge, corresponding to high PV gradients and outside the vortex (or surf zone) with small PV values. The limit of the vortex corresponds to the EL of maximum PV gradient, weighted by the wind module. Then this limit is smoothed temporally with a moving average of 5 days.

3.2 Methodology for classification

Nash criterion was already used in several studies to distinguish measurements (ozone profiles and total columns) inside and outside the vortex in the Southern Hemisphere (Godin et al., 2001; Bodeker et al., 2002; Pazmino et al., 2005, 2008; Kuttipurath et al., 2013, 2015). In the case of total columns, measurements were considered inside the vortex when their corresponding EL was larger than the EL of the vortex limit at a specific isentropic level (e.g. 550K, Bodeker et al., 2002; Pazmino et al., 2005). However this "standard" method does not take into account the baroclinicity of the vortex. It can result in the classification of total ozone columns inside the vortex while partial columns below or above the selected isentropic level are outside the vortex. The total ozone column may thus not represent the ozone behaviour inside the vortex. In order to consider possible vortex baroclinicity, another approach is used, where vortex classification at different isentropic levels is considered. For this second approach, the range of selected isentropic levels is chosen in the altitude region of maximum ozone depletion: from 400 K to 600 K with a step of 25K.

In order to illustrate the impact of vortex baroclinicity on the classification of total ozone column inside the vortex, Fig. 1 shows MSR-2 total ozone fields on October 7, 2012, with the vortex position computed at different isentropic levels superimposed. The vortex position curves are represented by black to light grey colours. On this particular day, region classified inside the vortex considering 400 K-600 K range is limited by the vortex position at 400K (black line) towards Antarctic West coast and Palmer Peninsula and by 600 K (light grey line) towards the Antarctic East coast. In the case of standard classification using a single level at 475 K or 550 K, the region estimated as inside the vortex consists in an area with total ozone columns higher than 400DU not considered in the classification using several isentropic levels between 400K and 600K. Regions where total ozone columns are lower than 220 DU are taken into account by the different classifications. A daily mean total ozone column of 213.4 DU was computed inside the vortex using new classification. Standard classification estimate 40 DU and 20 DU higher ozone mean at 475 K and 550 K respectively.

4 Vortex baroclinicity

Both methods of classification described in the previous section were applied to satellite composite total ozone data series SAT and MRS-2 reanalysis at each grid point. For each year, daily mean total ozone amount inside the vortex was averaged

over two periods: the whole month of September, and the period of maximum ozone depletion between September 15th and October 15th (15Sept-15Oct). Figure 2 shows the evolution of total ozone average inside the vortex for the 15Sept-15Oct period between 1980 and 2016 for SAT data series computed with the standard classification method based on single isentropic level (475 K and 550 K) and with the second method using the 400 K – 600 K range of levels. Error bars represent two sigma standard error (2σ). Similar interannual total ozone variability is observed for the time series obtained by the different methods. The correlation coefficients between the range method and the standard one at 475 K and 550 K are 0.976 and 0.995 respectively. Despite these good correlations, the data series are significantly different at 2σ level. Higher ozone values are found with the standard method, especially for the 475 K level, with a mean difference with the TOC ozone time series based on the range method of ~15 % over the whole analysis period. Three years stand out in the comparison: 1995, 1999 and 2011, during which the inside vortex region was systematically larger at 475 K compared to higher isentropic levels during the period. Similar results are observed for September (not shown). In this work, the second method is preferably used since it takes into account the ozone loss at different isentropic levels, which strongly impact the total column.

SAT total ozone time series obtained in September and 15Sep-15Oct with the range classification method are displayed in Figure 3. September presents ~7% higher ozone mean values than the 15Sept-15Oct period. Similar interannual variability is observed between the two periods as shown by the correlation coefficient of 0.97. The last three years present very similar ozone values around 200 DU in September while 15Sept-15Oct period shows larger variability.

MSR2 total ozone data series inside the vortex were compared to SAT series. Figure 4 illustrates the relative difference between MSR2 and SAT considering the 400K-600K range classification. Differences of about ±0.5% are observed in the 1980s. During the first decade of 1990s, a large variability fluctuating from -3% to 5% is found linked to SBUV averaged total ozone column. In fact, SBUV level 2 measurements do not allow a homogeneous sampling of the whole vortex as MSR-2. From 2001, differences are larger and generally positive, reaching ~5% in September and ~3% in 15Sept-15Oct. period. Overall, values in September present a mean bias of 1.4% (dash blue line in Fig. 4), and in 15Sept-15Oct a smaller bias value of 0.6% (dash red line in Fig. 4). Temporal evolution of the differences, e.g. negative trend in the 1980s and positive trend in the 2000s, can have an impact on the long-term ozone trends retrieved from both records.

In the next section, ozone data series using different classification method are used to evaluate the impact of vortex baroclinicity on ozone trends inside the vortex for both studied periods.

5 Trend analysis

5.1 Method

In order to evaluate ozone recovery in Antarctica, estimation of trends before and after 2001 were calculated using a multi-regression model (Nair et al., 2013) updated from AMOUNTS (Adaptative Model for Unambiguous Trend Survey) model (Hauchecorne et al., 1991; Kerzenmacher et al., 2006). Different common explanatory variables such as eddy heat flux (HF), solar flux (SF), Quasi-Biennial Oscillation (QBO), Aerosols (Aer), Antarctic Oscillation (AAO) are used to explain total ozone variability over 1980-2016 period. These proxies were widely applied in different trend studies (e.g. de Laat et al., 2015 and references herein). ODSs contribution on long-term trend of ozone can be stated by piece wise linear trend functions (PWLT). Total ozone variability (Y) can be expressed following Eq. (1):

$$Y(t) = \mathrm{K} + C_{HF}\mathrm{HF(t)} + C_{SF}\mathrm{SF(t)} + C_{QBO30}\mathrm{QBO30(t)} + C_{QBO10}\mathrm{QBO10(t)} + C_{Aer}\mathrm{Aer(t)} + C_{AAO}\mathrm{AAO(t)} + C_{GRAD}\mathrm{GRAD(t)} + \mathrm{PWT(t)} + \in (t), \quad (1)$$

Atmos. Chem. Phys. Discuss., https://doi.org/10.5194/acp-2017-1157
Manuscript under review for journal Atmos. Chem. Phys.
Discussion started: 12 December 2017

where t is the time in year from 1980 to 2016, K is a constant, C_{proxy} are the regression coefficients of the respective proxies mentioned above and ∈ (t) the total ozone residuals. Table 1 shows the respective information on each proxy: source, specific characteristics and time window where proxy values are averaged to represent the respective year value. QBO effect on ozone variability is estimated using two proxies at 30hPa (QBO30) and 10hPa (QBO10), which are out of phase by $\sim\frac{\pi}{2}$ (Steinbrecht et al., 2003). The HF proxy corresponds to the average over the August-September period of the 45-day mean Heat Flux in the 45°S-75°S latitude range at 70hPa from MERRA analyses. The time window of August-September is selected for computing the mean HF, following de Laat et al. (2015) recommendation to obtain the best regression results. For the Aer term, a merged proxy of monthly aerosol optical depth (AOD) is computed from updated Sato et al., (1993) dataset for the 1980-1990 period and from four satellite data series (SAGE II, OSIRIS, CALIOP and OMPS) for the 1991-2016 period. AOD datasets are averaged over the 40°S-65°S zonal region in the 15-30 km altitude range. Updated Sato et al. data are obtained from NASA monthly AOD at 550nm. The satellite AOD data over 1991-2016 period were computed at 532nm. The Sato et al. data set was converted to 532 nm according to Khaykin et al. (2017). The merged AOD proxy was obtained by normalizing the Sato et al. time series to the SAGE II data in December 1991. The regression code uses the AOD values in April before the complete formation of the vortex in order to avoid possible contamination of satellite data by Polar Stratospheric Clouds. The April AOD proxy is represented by a bold black line in Fig. 5 together with Sato et al. (1993) and satellites datasets for the 1991-2016 period. A new GRAD(t) proxy was developed to take into account the stability of the vortex during the studied period. This proxy corresponds to the maximum gradient of PV as a function of EL at 550 K during both studied periods (e.g. September and 15Sept-15Oct). It is calculated from ERA-Interim data. GRAD and HF proxies are detrended by removing a 3rd order polynomial fit to minimize correlation with PWLT proxies. Figure 6 displays GRAD and HF proxies before and after removing trends. An anti-correlation of 0.45 between these two proxies is observed with p-value <0.01, but the addition of GRAD proxy provides a much better agreement between measurements and model. The contribution of the GRAD(t) proxy to the improvement of the MLR results is discussed in Sect. 5.2.3.

For the long-term trends, two piecewise linear trend ($PWT(t) = C_{t1}\mathrm{t1(t)} + C_{t2}\mathrm{t2(t)}$) functions calculated before and after the turnaround year are usually used to estimate the change of slope in long-term evolution of ozone linked to ODS (e.g. Reinsel et al., 2002; Kuttipurath et al., 2013, de Laat et al., 2015). In this work a Modified PWLT model (PWT) is used to take into account the slower growth of ODS near the turnaround year and ozone loss saturation effect inside the vortex in October (Yang et al., 2008). The PWT model is represented by Eq. (2):

$$PWT(t) = C_{t11}\mathrm{t11(t)} + C_{t12}\mathrm{t12(t)} + C_{t2}\mathrm{t2(t)} \quad (2)$$

where C_{t11} and C_{t2} are the coefficients of the linear functions and C_{t12} of the parabolic function. First period is represented by a linear time proxy t11 and a parabolic time proxy t12. The second period is expressed only by a linear time proxy t2. The proxies are stated as follow:

$$\mathrm{t11} = \begin{cases} t & 0 < t \le T_0 \\ T_0 & T_0 < t \le T_{end} \end{cases} \quad (3)$$

$$\mathrm{t12} = \begin{cases} \left(t - \left(\frac{T_0+1}{2}\right)\right)^2 & 0 < t \le T_0 \\ \left(\frac{T_0-1}{2}\right)^2 & T_0 < t \le T_{end} \end{cases} \quad (4)$$

$$\mathrm{t2} = \begin{cases} 0 & 0 < t \le T_0 \\ t - T_0 & T_0 < t \le T_{end} \end{cases} \quad (5)$$

T_0 corresponds to the turnaround year in the considered period. In this work, 2001 was selected as turnaround year when equivalent effective stratospheric chlorine (EESC) maximizes for a mean age-of-air of 5.5yr (Newman et al., 2007). The corresponding value for T_0 is 22. T_{end} corresponds to the number of years considered in the study (37 for 1980-2016). The

minimum of the parabolic time proxy t12 is set to the middle of the period before turnaround year so that the slope of the proxy is zero on that year. In this case the coefficient of t11 (C_{t11}) can be considered as the linear trend before 2001. After 2001, t11 and t12 are constant and then the linear trend is given by t2 coefficient (C_{t2}). Figure 7 represents the evolution of the three piece-wise proxy anomalies normalised by the corresponding standard deviation.

5.2 Results

The multi-regression model described in previous section was applied to SAT and MSR-2 total ozone anomalies series (monthly total ozone – mean total ozone) of September and 15Sept.-15Oct. periods. Times series of total ozone data corresponding to the different classification methods described in Sect. 4 were used to evaluate the impact of vortex baroclinicity on total ozone trends.

5.2.1 September

A rapid decrease of ozone levels occurs within the polar vortex in Antarctica from the last two weeks of August to the end of September when the necessary sunlight to start the ozone catalytic destruction cycles is present again above austral polar regions. Important differences of total ozone levels are found inside the vortex between the first and second half of September. Very low values are specially observed during the last week. Despite total ozone variability during September, most recent studies were performed to detect the first signs of ozone recovery linked to ODS decrease since 2000 using multi-linear regression model on ground-based and satellite datasets or chemistry-climate / chemistry-transport models simulations (Solomon et al., 2016; Chipperfield et al., 2017; Weber et al., 2017). Those papers used data or simulations poleward ~60°S and conclude that first signs of recovery are highlighted in Antarctica for September but not yet on October due to larger dynamical variability during that month. In this work, results from our multi-regression model will be evaluated and compared to those previous works for the September period. In our study, trend estimation was performed before and after 2001 as described in the previous section. Figure 8 illustrates the results of the regressions model for the SAT total ozone data series inside the vortex using the 400K-600K range classification. The top panel represents the deseasonalized total ozone observations as well as the regressed ozone values. The model results reproduce quite well the interannual variability of measurements except in 2002 when the vortex split in two parts in late-September due to a major sudden stratospheric warming (e.g., Allen et al., 2003). Likewise, the year 2000 characterised by a large ozone hole area in September, presents a relatively high value of residual of ~20DU. Contributions of different proxies are shown in the second to fourth panels of Fig. 7. Fitted HF and GRAD were added (black line in second panel of Fig. 8) due to the correlation between both proxies. The model term linked to the HF+GRAD fitted proxy represents the second largest contribution to total ozone interannual variability (~10 % of the total variance) after the PWT proxy which contributes to about 80% of the total variability. Other contributions to interannual ozone variability (third panel of Fig. 8) represent only 1 %. Aerosol contribution of ~9 DU linked to Pinatubo in 1992 and ~6 DU due to El Chichon significantly helps HF+GRAD fitted proxy to explain ozone variation on those years. Negligible impact is seen in other years. Fitted QBO (QBO30hPa + QBO10hPa) explains ±5 DU. The contribution of SF and AAO proxies is negligible.

The model explains 93% of the ozone variability as deduced from the determination coefficient R^2. The estimated total ozone trends before and after 2001 are -5.55±0.71 DU yr^{-1} (-26.7±3.4 % $decade^{-1}$) and 1.87±1.18 DU yr^{-1} (9±5.7 % $decade^{-1}$), respectively. Both trends are significant (i.e. statistically different from zero) at 2σ. The 1980-2000 period presents higher depletion rate compared to Weber et al., 2017 (from -12 to -19% per decade depending on dataset) and comparable rate for 2001-2016 (8-10 % $decade^{-1}$). Comparable values of trends are found when 475 K classification level is used (-21.3±3.6 % $decade^{-1}$ and 11±5.9% $decade^{-1}$). The 400 K-600 K classification allows us to obtain the best agreement between observations and regressed values (higher R^2) and lower χ ($\sqrt{\sum_i (obs_i - mod_i)^2/(n-m)}$) of residuals. Those results are represented in Table 2 for SAT and for MSR-2 total ozone datasets inside the vortex and for the three classifications

analysed in this study. Similar results are observed between both data series. MSR-2 presents slightly higher trend values after 2001. Note that 2016 was not available in MSR-2 data. SAT dataset is shortened to 2015 to evaluate sensibility of our model to the year 2016. Similar results are found compared to MSR-2 but with slightly higher values of trends after 2001, still significant at 2σ. Despite trend values after 2001 for 475 K are systematically higher by about 35 % than for the 400 K-600 K range, trend results between both classifications are not significantly different at 2σ level, suggesting a limited effect of vortex baroclinicity on trend estimation. The different results in Table 2 generally present a ratio between trends before and after 2001 smaller than 3, similar to that of ODS trends before and after the peak. Thus the ozone recovery trend could be due to ODS decrease. Nonetheless this trend cannot be reliably associated to chemical processes only and other processes could also play a role.

Computed trends over the 2001-2016 September period obtained with our model range from 1.85 to 2.67 DU yr^{-1} for all cases studied. They are all significant at 2σ level. Solomon et al., (2016) found significant total ozone trend of 2.5±1.7 DU yr^{-1} in September from SBUV and ozonesonde observations and similar results from the chemistry+dynamics+volcanoes (Chem-Dyn-Vol) simulation (2.8±1.6 DU yr^{-1}) using the Whole-Atmosphere Community Climate Model (WACCM). Estimated total ozone trend when only chemistry is considered in the model (Chem-Only) correspond to only half of the final trend (1.3±0.1 DU yr^{-1}).

A simulation test was done to evaluate the pertinence of using other proxies than PWT, HF and GRAD since only these fitted proxies present significant regression coefficient values at 95 % confidence interval. Results are represented in Table 2. Slightly lower determination factor R^2 is computed if only PWT, HF and GRAD are considered for September and comparable residual and trends. MSR-2 data series have presented alike results.

5.2.2 September 15 to October 15

In order to confirm healing of the Antarctic ozone hole, it is important to evaluate trends for the period where lowest total ozone values are observed inside the vortex e.g. between September 15th and October 15th. The same analysis as for September is performed. Figure 9 illustrates the regressions model results for total ozone of SAT data series inside the vortex using the 400K-600K classification. The interannual variability of measurements is better represented by the model than in September, with R^2 of 0.95 (see also Table 3). As for the September regression, fitted HF and GRAD proxies (black line on second panel) represent together the second largest contribution to total ozone interannual variability (~13 % of the total variance) after the PWT proxy (~80%) and the last decade of measurement is correctly reproduced by the model. Significant trends of -5.86±0.6 DU yr^{-1} (-30.2±3.2 % $decade^{-1}$) and 1.27±1 DU yr^{-1} (6.8±5.6 % $decade^{-1}$) are estimated before and after 2001. Similar results are observed if a single level classification is used with higher trend values after 2001 for 475K. All trend results are comparable within ±2σ. MSR-2 presents similar results except for classification at 550 K where trend after 2001 is significant at only 1.8σ. Solar Flux, QBO, Antarctic Oscillation and Aerosol (third panel of Fig. 9) explain ~1 % of the total variance. QBO explains ±3 DU interannual variability and Aerosol signal amount to ~7 DU and ~5 DU linked to Pinatubo in 1992 and El Chichon in 1983. SF contribution varies from 4.5 DU during the maximum (except for the last solar cycle, ~1 DU) to -2.4 DU during the minimum. AAO represents negligible contribution. Same test as for September was performed where proxies of SF, QBO, AAO and Aerosol were removed from the linear regression. Results are presented in Table 3.

The different cases shown in Table 3 present significant trends at 2σ over the 1980-2000 period. Trends estimated on second period present slightly significant values at 2σ except for MSR-2 at 550 K. Ratios of computed trends before and after 2001 are higher than 3 in both total ozone data series. Computed trend with 400K-600K classification is comparable to the Chem-Only trend calculated by WACCM in Solomon et al., 2016. Whatever ozone depletion could be considered as well constrained by the period (15Sep-15Oct) and by the classification (400 K-600 K), no direct relationship to healing could be

deduced. In addition, the ratio between trends (before/after 2001) is higher than 3, threshold value to consider a recovery due to ODS decline.

5.2.3 Impact of GRAD proxy on trend estimation

The HF proxy represents the cumulative effect of wave activity on vortex stability (e.g. a high HF corresponds to a warmer vortex) that seems insufficient to represent total ozone variability over the last decade, especially in 2010 and 2012. The GRAD proxy was developed in order to consider also the vortex stability during the studied periods (e.g. September and 15Sept-15Oct.). Figure 10 highlights the improvement in the regressed values by using the GRAD proxy. It shows the residuals of the trend simulation with and without GRAD as explanatory variable in the model. SAT measurements inside the vortex applying 400 K-600 K classification were used for this study. Results for September and 15Sept-15Oct periods are shown in the top and bottom panels of Fig. 10 respectively. As shown in Table 1, the residuals' variance (χ) is significantly reduced with the addition of the GRAD proxy. The second panels of Figures 8 and 9, show that in some years HF and GRAD proxies are in phase as during 2009-2014 when GRAD intensifies the HF contribution to ozone variability. This improvement is especially visible for the years 2010 and 2012. When both proxies are anticorrelated, as in 2015 and 2016, the improvement linked to the GRAD proxy is also observed. As a further illustration, Table 2 and 3 show the results of the regressions excluding GRAD proxy for September and 15Sept-15Oct respectively. The determination coefficient is generally reduced by ~0.05 and χ values are higher by 20 % to 35 %. Computed trends before and after 2001 show lower and higher trends in absolute values respectively but within $\pm 2\sigma$ of initial trend results including the GRAD proxy. Trends over the 2001-2016 period estimated without the GRAD proxy are still significant at 2σ in September but only at 1.8σ for the 15Sept-15Oct.

6. Temporal evolution of low total ozone values inside the vortex

The ozone hole is defined as the region with total ozone columns lower than 220 DU. This standard value was used in different studies to evaluate the ozone depletion from the Ozone Hole Area (OHA) (e.g. Newman et al., 2006; Solomon et al., 2016) or the Ozone Mass Deficit (OMD) (e.g. de Laat and van Weele, 2011) metrics. In this work, the relative daily area inside the vortex with values lower than different threshold levels is computed and integrated over different periods (September, 15Sept-15Oct and October). Figure 11 shows the relative area with respect to the vortex's area of these low values relative to three different thresholds: 220 DU, 150 DU and 125 DU, for the 15Sept-15Oct period. MSR-2 and TOMS/OMIT datasets are used and vortex area is estimated with the 400 K-600 K range classification, the results of previous sections having shown that the range classification better constrains the ozone hole area. Relative areas at 220 DU of both satellite datasets are similar. They show increasing amounts during the 1980s, a stabilisation in the 1990s and a higher inter-annual variability since 2001. The evolution of relative areas of MSR-2 with respect to 125DU and 150DU thresholds presents lower values than TOMS-EP/OMIT data. Nevertheless comparable inter-annual variability is observed. In contrast to 220 DU relative areas, the evolution of relative areas to 150DU and 125DU shows a delayed increase from the mid-1980s and mid-1990s respectively, reaching a maximum in both cases in 2000 and a steady decrease from 2006, with very large inter-annual variability from 2000. In the three thresholds cases, several anomalous years are observed with important reduction of ozone depletion: 1988, 1991, 2002, 2004, 2010 and 2012. Note that these years correspond to a high contribution of HF+GRAD proxies to the regressed ozone values (Fig. 10, second panel). If we exclude the anomalous years, the 220 DU relative area corresponds to about 90% of the total vortex in average since 1990. In the most recent years, 125 DU and 150 DU relative areas decrease to less than 10% and 30% respectively of the vortex area from their peak value of 2000.

Solomon et al. (2016) have shown a slow delay in the formation of the ozone hole after 2000. This shift can be explained by the slower ozone loss rate after polar sunrise due to ODS decrease in the polar stratosphere. In this work, a possible time shift was investigated by comparing relative area inside the vortex lower than 220 DU in September, 15Sept-15Oct and October (Fig. 12). Higher relative area is observed in the 1980s in October, followed by 15Sept-15Oct and much smaller values for September. At the end of 1980s and 1990s, 15Sept-15Oct presents the higher relative area and in 2000s it shows similar area as in September. Since 2010, October areas are similar to those in 15Sept-15Oct, while September areas show increasingly smaller values. This divergence could be explained by a delay in the full formation of the ozone hole in September.

7 Conclusions

Two satellite based data series have been used to evaluate total ozone trends within the Southern polar vortex over the 1980-2016 period. A multi-regression model is applied to ozone values averaged over the September month and the 15 September to 15 October period in order to compute trends before and after the maximum of EESC in the polar stratosphere that occurred in 2001 (Newman et al., 2007). Proxies and time windows for averaging them are selected following de Laat et al. (2015) work.

Different methods to classify total ozone measurements inside the vortex are used in order to evaluate the impact of vortex baroclinicity on trend analysis. The total ozone time series using single level (475 K or 550 K) for classification show systematic differences compared to 400 K–600 K classification range but their inter-annual variability is similar with R>0.97 for both cases. Trends estimation results in higher absolute values using the Nash et al. criterion at 475K level compared to 550K level or the more restrictive condition based on the 400 K-600 K altitude range. However the corresponding computed trends are not significantly different at 2σ level.

A new proxy representing the vortex stability over the studied periods (September and 15Sept–15Oct), the GRAD proxy, is used in the multilinear regressions. This proxy improves the representation of total ozone inter-annual variability by the regressed values, with ~0.5 higher value for the R^2 determination coefficient and lower residuals for the different classification methods and datasets. The contribution of GRAD is particularly important since 2010. For the various time series and classification criteria used in this study, the best agreement between observations and regressed values is found for the 15Sept-15Oct period with higher R^2 coefficients.

Comparable negative trends before 2001 ranging from -4.9 DU.yr^{-1} to -5.6 DU yr^{-1} significant at 2σ levels are obtained for both periods (Sept and 15Sept-15Oct), and for the different data series and vortex classifications. Significant positive trends after 2001 of 2.2 DU.yr^{-1} in average are obtained for the September time series for all data sets, classification methods and regression analyses. The ratio between trends before and after 2001 is smaller than 3, in line with the slower decrease of ODS amounts in the stratosphere after the turnaround year. Despite this, it is not possible to ensure that the estimated trends are only due to ODS evolution. Regarding the 15Sept-15Oct period when ozone depletion is larger, retrieved trends are smaller with an average of 1.4 DU.yr^{-1} for all studied cases. In contrast to the September trends, the ratio before and after 2001 is generally larger than 3. The trends are slightly significant at 2 sigma level except for the classification at 550K. The best trend model applied on the data using the 400K-600 K range classification method shows increasing trends of respectively 1.27 ±1.0 DU.yr-1 and 1.18±1.12 DU.yr-1 for the SAT and MSR-2 records.

Polar ozone recovery was also evaluated by examining the evolution of low ozone values within the vortex. Areas with values lower than 125, 150 and 220 DU relative to the vortex area were computed using both datasets and the 400K-600K classification. For the 125 and 150 DU thresholds, relative areas show a steady decrease since the beginning of the 21st century, while for the 220 DU threshold, the relative area evolution is more stable. All three relative area curves are marked by increased variability since 2000.

The delay in the formation of the ozone hole can be evaluated by comparing the 220 DU relative areas for the September, 15-Sept-15Oct, and October periods. October (September) areas showed the largest (lowest) values until 1987. After that year, the evolution of the curves was inverted and the largest relative areas were generally observed in September (88 % in average of the polar vortex occupied by total ozone columns lower than 220 DU) until the first decade of 2000s. Since 2010, October relative areas are similar to those of the 15Sept-15Oct period, with still more than 75 % of the vortex characterized by total ozone levels less than 220 DU in most of the years. These results confirm Solomon et al. (2016) findings on the delay in the formation of the Antarctic ozone hole in September.

In summary, this work shows clear signs of ozone recovery in September with significant trend values at 2σ and smaller but still significant increasing trends in the 15Sept-15Oct period, when ozone depletion is highest. Recovery in October is confirmed by the very low ozone values (below 150 DU) within the vortex since 2010. Comparison of ozone hole areas in September and October confirm the later formation of the ozone hole in September.

Data availability. The source of the different total ozone column datasets and classical proxy time series utilised in this work are publically available from the websites given in the text and in Table 1. The satellite data used to build the Aerosol proxy are available at https://eosweb.larc.nasa.gov/project/calipso/calipso_table for CALIPSO; https://eosweb.larc.nasa.gov/project/sage2/sage2_table for SAGE II, http://odin-osiris.usask.ca/ for OSIRIS; http://mls.jpl.nasa.gov/products/h2o_product.php for MLS; and https://ozoneaq.gsfc.nasa.gov/data/omps/ for OMPS V1 LP. Other data as equivalent latitude and GRAD proxy are available upon request.

Competing interests. The authors declare that they have no conflict of interest.

Acknowledgements. The authors thank NASA/GSFC and TEMIS for total ozone column data of TOMS/SBUV/OMI-TOMS and MSR-2, respectively. They are grateful to Cathy Boone of ESPRI data centre of Institut Pierre Simone Laplace (IPSL) to provide ERA interim data. This work was supported by the Dynozpol project funded by the French Institut National des Sciences de l'Univers (INSU) of the Centre National de la Recherche Scientifique (CNRS).

References

Allen, D., Bevilacqua, R., Nedoluha, G., Randall, C., and Manney, G.: Unusual stratospheric transport and mixing during 2002 Antarctic winter, Geophys. Res. Lett., 30, 1599, doi: 10.1029/2003GL017117, 2003.

Bhartia, P. K., and Wellemeyer C.: TOMS-V8 total O3 algorithm, in OMI Algorithm Theoretical Basis Document , vol. II, OMI Ozone Products, edited by P. K. Bhartia, pp. 15–31, NASA Goddard Space Flight Center, Greenbelt, Maryland, USA., 2002.

Bodeker, G. E., Struthers, H., and Connor, B. J.: Dynamical containment of Antarctic ozone depletion, Geophys. Res. Lett., 29(7), 1098, doi:10.1029/2001GL014206, 2002.

Chipperfield, M, Bekki, S., Dhomse, S, Harris, N. R. P., Hassler, B., Hossaini, R, Steinbrecht, W., Thiéblemont, R., and Weber M.: Detecting recovery of stratospheric ozone layer, Nature, 549, 211–218, doi:10.1038/nature23681, 2017.

Chubachi, S.: A special observation at Syowa station, Antarctica from February 1982 to January 1983, in: Atmospheric Ozone, edited by: Zerefos, C. and A. Ghazi, Springer Netherlands, 285-289, doi:0.1007/978-94-009-5313-0_58, 1985.

Farman, J. C., Gardiner, B. G., and Shanklin, J. D.: Large losses of total ozone in Antarctica reveal seasonal ClOx/NOx interaction, Nature, 315, 207–210, doi:10.1038/315207a0, 1985.

de Laat, A. T. J., van der A, R. J., and van Weele, M.: Tracing the second stage of ozone recovery in the Antarctic ozone-hole with a "big data" approach to multivariate regressions, Atmos. Chem. Phys., 15, 79-97, doi:10.5194/acp-15-79-2015, 2015.

de Laat, A. T. J. and van Weele, M.: The 2010 Antarctic ozone hole: Observed reduction in ozone destruction by minor sudden stratospheric warmings, Sci. Rep., 1, 38, doi:10.1038/srep00038, 2011.

Dee, D.P., Uppala, S. M., Simmons, A. J., Berrisford, P., Poli, P., Kobayashi, S., Andrae, U., Balmaseda, M. A., Balsamo, G., Bauer, P., Bechtold, P., Beljaars, A. C. M., van de Berg, L., Bidlot, J., Bormann, N., Delsol, C., Dragani, R., Fuentes, M., Geer, A. J., Haimberger, L., Healy, S. B., Hersbach, H., Hólm, E. V., Isaksen, L., Kållberg, P., Köhle.r, M., Matricardi, M., McNally, A. P., Monge-Sanz, B. M.,

Morcrette, J.-J., Park, B.-K., Peubey, C., de Rosnay, P., Tavolato, C., Thépaut, J.-N., and Vitart, F.: The ERA-Interim reanalysis: configuration and performance of the data assimilation system. Q. J. R. Meteorol. Soc., 137, 553-597, doi:10.1002/qj.828, 2011.

Frederick, J. E., Cebula, R. P., and Heath, D. F.: Instrument characterization for the detection of long-term changes in stratospheric ozone: An analysis of the SBUV/2 radiometer, J. Atmos. Oceanic Technol., 3, 472–480, doi:10.1002/jgrd.50503, 1986.

Godin, S., Bergeret, V., Bekki, S., David, C., and Mégie, G.: Study of the interannual ozone loss and the permeability of the Antarctic polar vortex from aerosols and ozone lidar measurements in Dumont d'Urville (66.4°S, 140°E), J. Geophys. Res., 106(D1), 1311-1330, doi:10.1029/2000JD900459, 2001.

Hauchecorne, A., Chanin, M.-L., and Keckhut, P.: Climatology and trends of the middle atmospheric temperature (33-87 km) as seen by Rayleigh lidar over the south of France. J. Geophys. Res., 96, 15297–15309, doi:10.1029/91JD01213,1991.

Hauchecorne, A., Godin, S., Marchand, M., Heese, B., and Souprayen, C.: Estimation of the Transport of Chemical Constituents from the Polar Vortex to Middle Latitudes in the Lower Stratosphere using the High-Resolution Advection Model MIMOSA and Effective Diffusivity, J. Geophys. Res., 107(D20), 8289, doi:10.1029/2001JD000491, 2002.

Kerzenmacher, T. E., Keckhut, P., Hauchecorne, A., and Chanin, M.-L.: Methodological uncertainties in multi-regression analyses of middle-atmospheric data series, J. Environ. Monit., V8, 7, 682-690, doi: 10.1039/B603750J, 2006.

Khaykin, S.M., Godin-Beekmann, S., Keckhut, P., Hauchecorne, A., Jumelet, J., Vernier, J.-P., Bourassa, A., Degenstein, D.A., Reiger, L.A., Bingen, C., Vanhellemont, F., Robert, C., DeLand, M., and Bhartia, P.K., Variability and evolution of mid-latitude stratospheric aerosol budget from 22 years of ground-based lidar and satellite observations, Atmos. Chem. Phys., 17, 1829–1845, doi:105194/acp-17-1829-2017, 2017.

Kuttippurath, J., Goutail, F., Pommereau, J.-P., Lefèvre, F., Roscoe, H. K., Pazmino, A., Feng, W., Chipperfield, M. P., and Godin-Beekmann, S.: Estimation of Antarctic ozone loss from ground-based total column measurements, Atmos. Chem. Phys., 10, 6569–6581, doi:10.5194/acp-10-6569-2010, 2010.

Kuttippurath, J., Lefèvre, F., Pommereau, J.-P., Roscoe, H.K., Goutail, F., Pazmino, A., and Shanklin, J.D.: Antarctic ozone loss in 1979–2010: first sign of ozone recovery, Atmos. Chem. Phys., 13, doi:10.5194/acp-13-1625-2013, 1625-1635, 2013.

Kuttippurath, J., Godin-Beekmann, S., Lefèvre, F., Santee, M. L., Froidevaux, L., and Hauchecorne, A.: Variability in Antarctic ozone loss in the last decade (2004–2013): High-resolution simulations compared to Aura MLS observations. Atmos. Chem. Phys. 15, 10385–10397, doi:10.5194/acp-15-10385-2015, 2015.

Lefèvre, F., Brasseur, G. P., Folkins, I., Smith, A. K., and Simon, P.: Chemistry of the 1991–92 stratospheric winter: three dimensional model simulations, J. Geophys. Res., 99, 8183–8195, doi:10.1029/93JD03476, 1994.

Levelt, P. F., van den Oord, G. H. J., Dobber, M. R., Mälkki, A., Visser, H., de Vries, J., Stammes, P., Lundell, J. O. V. and Saari, H.: The Ozone Monitoring Instrument, IEEE Trans. Geosci. Remlote Sens., vol. 44, 5, 1093-1101, May 2006.

McIntyre, M. and Palmer, T.: The 'surf zone' in the stratosphere, J. Atmos. Terr. Phys., 46, 825–849, doi:10.1016/0021-9169(84)90063-1, 1984.

McPeters R.D, Krueger, A.J., Bhartia, P.K., Herman, J.R., Wellemeyer, C. G., Seftor, C. J., Jaross, G., Torres, O., Moy, L., Labow, G., Byerly, W., Taylor, S. L., Swissler, T., and Cebula, R. P.: Earth Probe Total Ozone Mapping Spectrometer (TOMS) Data Products User's Guide, NASA Reference Publication 1998-206895, NASA, Washington DC, 1998.

McPeters, R., Kroon, M., Labow, G., Brinksma, E., Balis, D., Petropavlovskikh, I., Veefkind, J. P., Bhartia, P. K., and Levelt, P. F.: Validation of the Aura Ozone Monitoring Instrument total column ozone product, J. Geophys. Res., 113, D15S14, doi:10.1029/2007JD008802, 2008.

McPeters, R. D., Bhartia, P. K., Haffner, D., Labow, G. J., and Flynn L.: The version 8.6 SBUV ozone data record: An overview, J. Geophys. Res. Atmos., 118, 8032–8039, doi:10.1002/jgrd.50597, 2013.

Nair, P.J., Godin-Beekmann S., Kuttippurath J., Ancellet G., Goutail F., Pazmino A., Froidevaux L., Zawodny J.M., Evans R.D., Wang H.J., J. Anderson, J., and Pastel, M.: Ozone trends derived from the total column and vertical profiles at a northern mid-latitude station, Atmospheric Chemistry and Physics, 13, 20, 10373-1038, doi:10.5194/acp-13-10373-2013, 2013.

Nash, E. R., Newman, P. A., Rosenfield, J. E., and Schoeberl, M. R.: An objective determination of the polar vortex using Ertel's potential vorticity, J. Geophys. Res., 101, 9471–9478, doi:10.1029/96JD00066, 1996.

Newman, P. A., Nash, E. R., Kawa, S. R, Montzka, S. A., and Schauffler, S. M.: When will the Antarctic ozone hole recover?, Geophys. Res. Lett., 33, L12814, doi:10.1029/2005GL025232, 2006.

Newman, P. A., Daniel, J. S., Waugh, D. W., and Nash, E. R.: A new formulation of equivalent effective stratospheric chlorine (EESC), Atmos. Chem. Phys., 7, 4537-4552, doi:10.5194/acp-7-4537-2007, 2007.

Pazmino A. F., Godin-Beekmann, S., Ginzburg, M., Bekki, S., Hauchecorne, A., Piacentini, R., and Quel, E.: Impact of Antarctic polar vortex occurrences on total ozone and UVB radiation at southern Argentinean and Antarctic stations during 1997–2003 period, J. Geophys. Res., 110, D03103, doi:10.1029/2004JD005304, 2005.

Pazmino, A. F., Godin-Beekmann, S., Luccini, E. A. , Piacentini, R. D., Quel, E. J., and Hauchecorne, A.: Increased UV radiation due to polar ozone chemical depletion and vortex occurrences at southern sub-polar latitudes in the period [1997–2005], Atmos. Chem. Phys., 8, 5339–5352, doi:10.5194/acp-8-5339-2008, 2008.

Reinsel, G. C., Weatherhead, E. C., Tiao, G. C., Miller, A. J;, Nagatani, R. M., Wuebbles, D. J., and Flynn, L. E.: On detection of turnaround and recovery in trend for ozone, J. Geophys. Res., 107(D10), 4078, doi:10.1029/2001JD000500, 2002.

Salby, M.L., Titova, E.A., and Deschamps, L.: Changes of the Antarctic ozone hole: Controlling mechanisms, seasonal predictability, and evolution, J. Geophys. Res., 117, D10111, doi:10.1029/2011JD016285, 2012.

Solomon, S., Ivy, D. J., Kinnison, D., Mills, M. J., Neely, R. R., and Schmidt, A.: Emergence of healing in the Antarctic ozone layer, Science, doi:10.1126/science.aae0061, 2016.

Steinbrecht, W., Hasslet, B., Claude, H., Winkler, P., and Storlarski, R. S.: Global distribution of total ozone and lower stratospheric temperature variations, Atmos. Chem. Phys., 3, 1421-1438, doi:10.5194/acp-3-1421-2003, 2003.

van der A, R. J., Allaart, M. A. F., and Eskes, H. J.: Extended and refined multi sensor reanalysis of total ozone for the period 1970–2012, Atmos. Meas. Tech., 8, 3021-3035, https://doi.org/10.5194/amt-8-3021-2015, 2015.

Weber, M., Coldewey-Egbers, M., Fioletov, V. E., Frith, S. M, Wild, J. D., Burrows, J. P., Long, C. S., and Loyola., D.: Total ozone trends from 1979 to 2016 derived from five merged observational datasets - the emergence into ozone recovery, Atmos. Chem. Phys. Discuss, https://doi.org/10.5194/acp-2017-853, 2017.

WMO (World Meteorological Organization): Scientific assessment of ozone depletion: 2006, Global Ozone Research and Monitoring Project-Report 50, Geneva, Switzerland, 2007.

WMO (World Meteorological Organisation): Scientific assessment of ozone depletion: 2010, Global Ozone Research and Monitoring Project, Report 52, 516 pp., Geneva, Switzerland, 2011.

WMO (World Meteorological Organization): Scientific Assessment of Ozone Depletion: 2014, Global Ozone Research and Monitoring Project, Report No. 55, 416 pp., Geneva, Switzerland, 2014.

Yang, E.-S., Cunnold, D. M., Newchurch, M. J., Salawitch, R. J.; McCormick, M. P., Russell, J. M., Zawodny, J. M., and Oltmans, S. J.: First stage of Antarctic ozone recovery, J. Geophys. Res., 113, D20308, doi:10.1029/2007JD009675, 2008.

Atmos. Chem. Phys. Discuss., https://doi.org/10.5194/acp-2017-1157
Manuscript under review for journal Atmos. Chem. Phys.
Discussion started: 12 December 2017

Atmospheric Chemistry and Physics Discussions

Table 1: Information of proxies (source, characteristics and time window for the mean yearly value).

Proxy	Source	Characteristics	Time window
HF	NASA/Goddard Space Flight Center https://acd-ext.gsfc.nasa.gov/Data_services/met/ann_data.html	45-Day Mean Heat Flux between 45°S-75°S at 70hPa from MERRA	Aug.-Sept.
SF	Dominion Radio Astrophysical Observatory (National Research Council Canada) ftp://ftp.geolab.nrcan.gc.ca/data/solar_flux/monthly_averages/solflux_monthly_average.txt	Monthly averages of Solar Flux at 10.7cm wavelength	Sept.
QBO	Institute of Meteorology (Freie Universität Berlin) http://www.geo.fu-berlin.de/en/met/ag/strat/produkte/qbo	Monthly mean Quasi-Biennial Oscillation at 30 and 10hPa	Sept.
Aer	1980-1990: NASA/Goddard Space Flight Center https://data.giss.nasa.gov/modelforce/strataer/	AOD@550nm, 15-30km, 40°S-65°S zonal mean.	April
	Jan. 1991 – Nov. 2016 composite data series	AOD@532nm merged satellite time series of SAGE II, OSIRIS, CALIOP and OMPS following method described in Khaykin et al. (2017) 15-30km, 40°S-65°S zonal mean	
AAO	NOAA/National Weather Service ftp://ftp.cpc.ncep.noaa.gov/cwlinks/	Daily AAO index	Same as O3
GRAD		Daily maximum of PV slope at 550K computed from ERA-Interim data	Same as O3

Atmos. Chem. Phys. Discuss., https://doi.org/10.5194/acp-2017-1157
Manuscript under review for journal Atmos. Chem. Phys.
Discussion started: 12 December 2017

Atmospheric Chemistry and Physics Discussions

Table 2: Coefficient of determination R^2, trends ± 2σ in DU yr^{-1} before and after the turnaround year 2001 derived from multi-regression model using as input SAT (1980-2016) and MSR-2 (1980-2015) total ozone anomalies inside the vortex for September using three classification methods described in Sect. 3.2. The residual is represented in DU by $\chi = \sqrt{\sum_i (obs_i - mod_i)^2/(n-m)}$ where obs_i and mod_i correspond to observations and model monthly mean, n the number of years and m the number of parameters fitted as in Weber et al. (2017)

	Composite satellite data (SAT)			Multi-Sensor Reanalysis (MSR-2)		
	400 K-600 K	475 K	550 K	400 K-600 K	475 K	550 K
R^2	0.93	0.89	0.91	0.92	0.90	0.91
Trend before 2001	-5.55±0.71	-4.99±0.83	-5.35±0.75	-5.36±0.71	-4.99±0.78	-5.27±0.75
Trend after 2001	1.87±1.18	2.57±1.38	1.85±1.24	1.97±1.25	2.67±1.38	2.02±1.32
χ	11.44	13.37	12.00	11.33	12.49	12.02
Without SF, QBO, AAO and Aerosols						
R^2	0.92	0.88	0.89	0.91	0.89	0.89
Trend before 2001	-5.57±0.67	-5.07±0.76	-5.34±0.74	-5.34±0.67	-5.05±0.72	-5.23±0.75
Trend after 2001	1.96±1.07	2.51±1.21	2.01±1.17	2.07±1.16	2.67±1.25	2.15±1.31
χ	11.10	12.58	12.21	11.06	11.90	12.46
Without GRAD						
R^2	0.88	0.83	0.86	0.87	0.83	0.86
Trend before 2001	-5.44±0.91	-4.87±1.02	-5.24±0.93	-5.23±0.89	-4.84±0.99	-5.15±0.91
Trend after 2001	2.27±1.48	2.99±1.67	2.24±1.52	2.16±1.57	2.88±1.74	2.21±1.61
χ	14.55	16.40	14.92	14.31	15.83	14.63

Atmos. Chem. Phys. Discuss., https://doi.org/10.5194/acp-2017-1157
Manuscript under review for journal Atmos. Chem. Phys.
Discussion started: 12 December 2017

Atmospheric Chemistry and Physics Discussions

Table 3: Idem Table 2 for Sept15-Oct15 period.

	Composite satellite data (SAT)			**Multi-Sensor Reanalysis (MSR-2)**		
	400K-600K	475K	550K	400K-600K	475K	550K
R^2	0.95	0.94	0.94	0.95	0.94	0.94
Trend before 2001	-5.86±0.60	-5.56±0.68	-5.60±0.66	-5.84±0.63	-5.61±0.70	-5.64±0.71
Trend after 2001	1.27±1.00	1.78±1.14	1.21±1.01	1.18±1.12	1.72±1.24	1.15±1.26
χ	9.68	10.95	10.59	10.07	11.11	11.31
Without SF, QBO, AAO and Aerosols						
R^2	0.94	0.93	0.93	0.94	0.93	0.92
Trend before 2001	-5.88±0.58	-5.67±0.66	-5.60±0.64	-5.84±0.60	-5.71±0.65	-5.63±0.69
Trend after 2001	1.06±0.93	1.37±1.05	1.05±1.03	1.08±1.04	1.42±1.13	1.07±1.19
χ	9.62	10.94	10.67	9.87	10.77	11.36
Without GRAD						
R^2	0.91	0.89	0.90	0.91	0.89	0.90
Trend before 2001	-5.73±0.80	-5.42±0.88	-5.48±0.83	-5.67±0.82	-5.43±0.90	-5.48±0.86
Trend after 2001	1.56±1.33	2.08±1.46	1.48±1.37	1.32±1.47	1.88±1.61	1.29±1.53
χ	12.96	14.21	13.34	13.21	14.45	13.78

Atmos. Chem. Phys. Discuss., https://doi.org/10.5194/acp-2017-1157
Manuscript under review for journal Atmos. Chem. Phys.
Discussion started: 12 December 2017

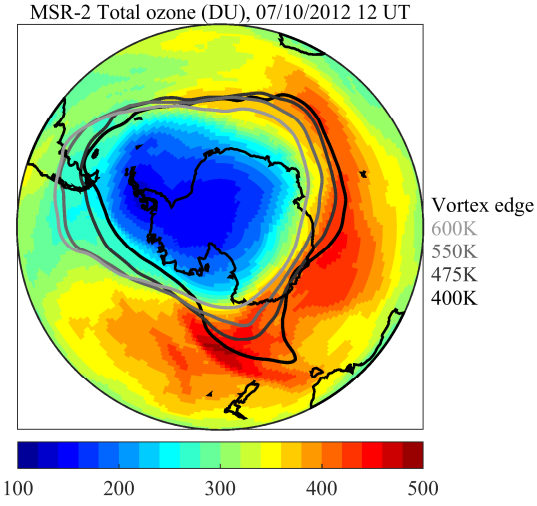

Figure 1: Total ozone (DU) from MSR-2 on October 7, 2012 at 12 UT. Vortex edge position at different isentropic levels are auditioned to the map and represented by black to light grey lines.

Atmos. Chem. Phys. Discuss., https://doi.org/10.5194/acp-2017-1157
Manuscript under review for journal Atmos. Chem. Phys.
Discussion started: 12 December 2017

Atmospheric Chemistry and Physics Discussions

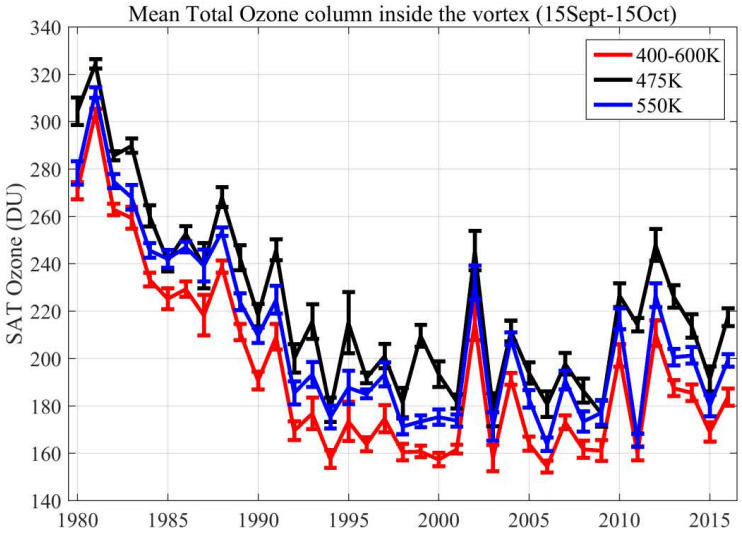

Figure 2: Evolution of total ozone of satellite composite (SAT) measurements inside the vortex averaged each year on 15Sept–15Oct period for different classifications: standard method at 475K and 550K represented by black and blue lines, respectively and method considering the 400-600K altitude range by red line. Error bars represent twice the standard error.

5

Atmos. Chem. Phys. Discuss., https://doi.org/10.5194/acp-2017-1157
Manuscript under review for journal Atmos. Chem. Phys.
Discussion started: 12 December 2017

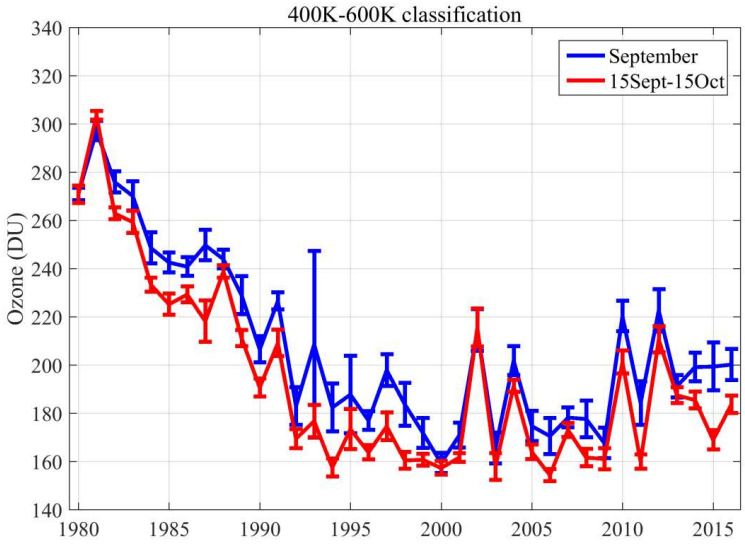

Figure 3: As in Fig. 2 but only for 400K-600K classification on different periods: September and mid-September to mid-October. Error bars represent 2σ.

Atmos. Chem. Phys. Discuss., https://doi.org/10.5194/acp-2017-1157
Manuscript under review for journal Atmos. Chem. Phys.
Discussion started: 12 December 2017

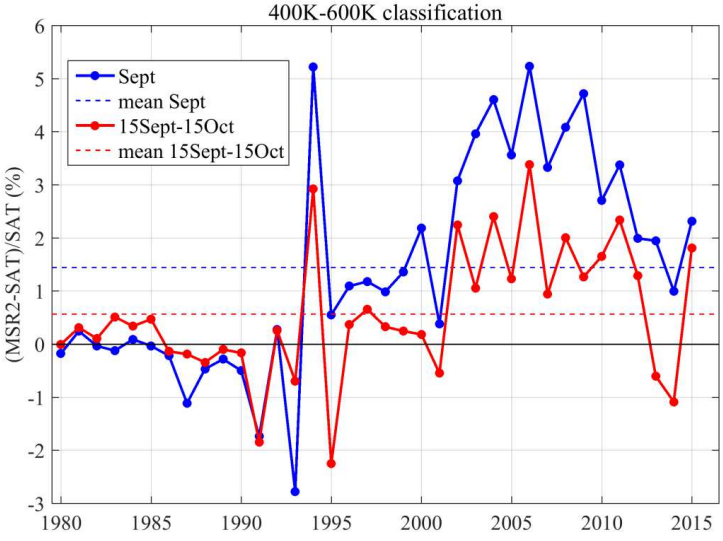

Figure 4: Relative difference between MSR2 and SAT mean total ozone inside the vortex for September (blue curve) and 15Sept-15Oct (red curve) periods. Horizontal dash lines correspond to the mean bias between data series.

5

Atmos. Chem. Phys. Discuss., https://doi.org/10.5194/acp-2017-1157
Manuscript under review for journal Atmos. Chem. Phys.
Discussion started: 12 December 2017

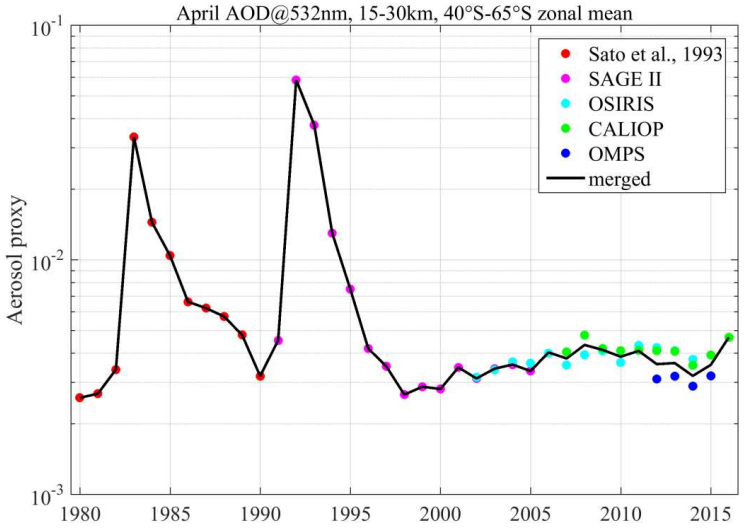

Figure 5: Time series of April monthly mean AOD at 532nm within 40°S-65°S and 15-30km of normalised Sato et al., 1993 dataset (see main text) and from satellites (SAGE II, OSIRIS, CALIOP, OMPS). The corresponding merged data is represented by the bold line.

Atmos. Chem. Phys. Discuss., https://doi.org/10.5194/acp-2017-1157
Manuscript under review for journal Atmos. Chem. Phys.
Discussion started: 12 December 2017

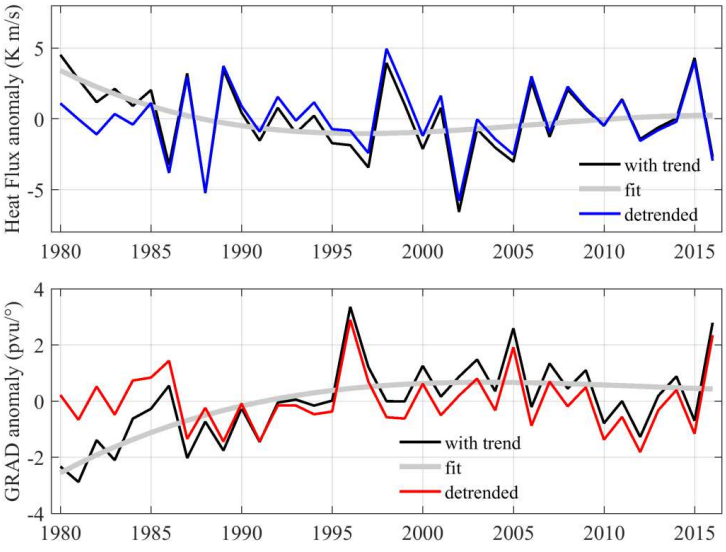

Figure 6: Heat Flux (top panel) and Gradient - GRAD (bottom panel) anomalies: before removing a polynomial fit of 3rd order (black line), fit (grey line) and after removing the fit (blue/red line).

Atmos. Chem. Phys. Discuss., https://doi.org/10.5194/acp-2017-1157
Manuscript under review for journal Atmos. Chem. Phys.
Discussion started: 12 December 2017

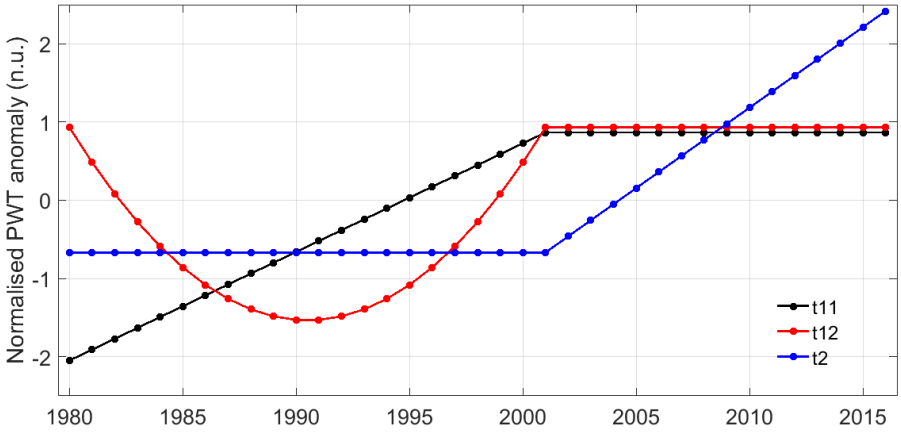

Figure 7: Anomalies of the linear functions before and after 2001 (t11 and t2, respectively) and parabolic function (t12) that correspond to the PWT proxy (see Eq. 2 to 5). Each proxy anomaly is normalised by the corresponding standard deviation.

Atmos. Chem. Phys. Discuss., https://doi.org/10.5194/acp-2017-1157
Manuscript under review for journal Atmos. Chem. Phys.
Discussion started: 12 December 2017

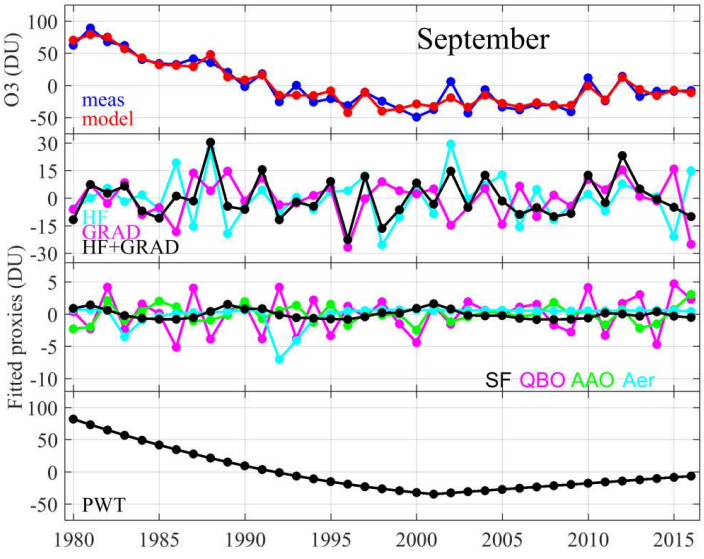

Figure 8: Deseasonalised total ozone inside the vortex of SAT series (meas) and regression model (model) for September using 400K-600K classification (top panel). Contributions of proxies are also shown: Heat Flux - HF, gradient - GRAD and the combination of both HF+GRAD (second panel); solar flux - SF, QBO (QBO at 30hPa + QBO at 50hPa), Antarctic Oscillation - AAO and Aerosol - Aer (third panel); and PWLT (bottom panel). Ozone anomalies and contributions of proxies are given in DU.

Atmos. Chem. Phys. Discuss., https://doi.org/10.5194/acp-2017-1157
Manuscript under review for journal Atmos. Chem. Phys.
Discussion started: 12 December 2017

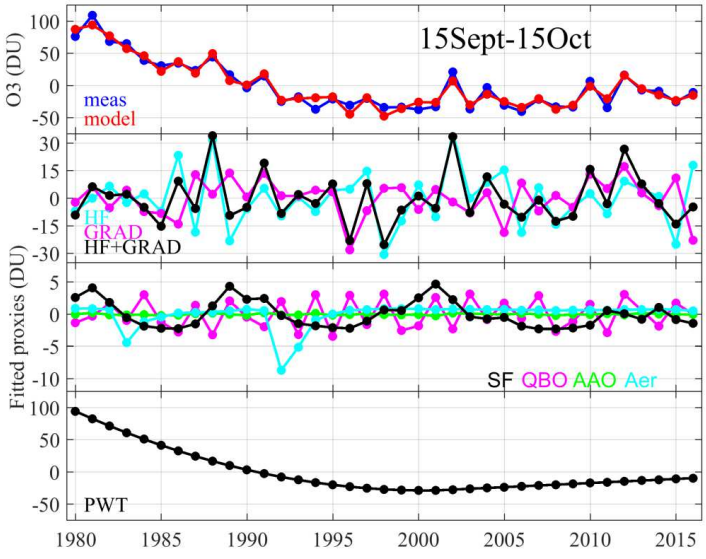

Figure 9: As in Fig. 7 for 15Sept-15Oct.

Atmos. Chem. Phys. Discuss., https://doi.org/10.5194/acp-2017-1157
Manuscript under review for journal Atmos. Chem. Phys.
Discussion started: 12 December 2017

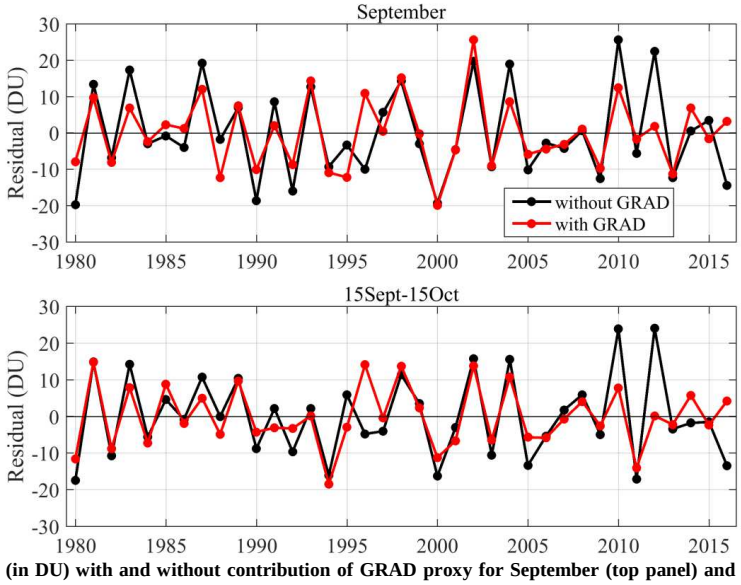

Figure 10: Residual (in DU) with and without contribution of GRAD proxy for September (top panel) and 15Sept-15Oct period (bottom panel)

Atmos. Chem. Phys. Discuss., https://doi.org/10.5194/acp-2017-1157
Manuscript under review for journal Atmos. Chem. Phys.
Discussion started: 12 December 2017

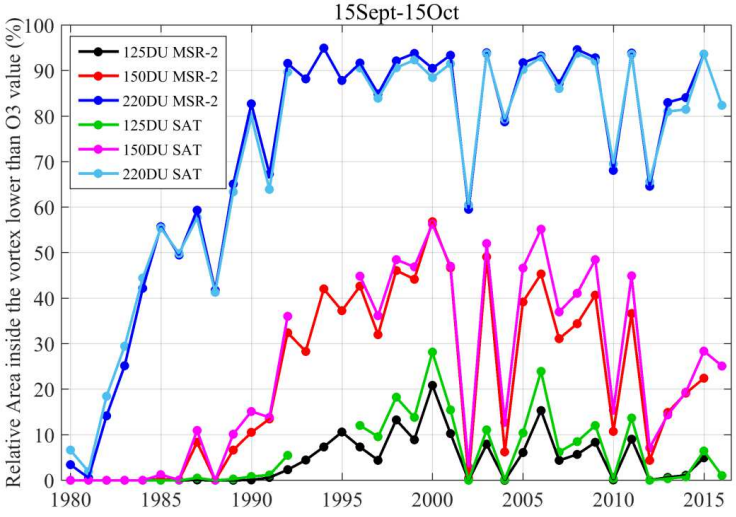

Figure 11: Relative area inside the vortex (in %) with values lower than 3 level thresholds (125, 150 and 220 DU) computed from MSR-2 and TOMS/OMIT datasets using 400K-600K classification on 15Sept-15Oct period.

5

Atmos. Chem. Phys. Discuss., https://doi.org/10.5194/acp-2017-1157
Manuscript under review for journal Atmos. Chem. Phys.
Discussion started: 12 December 2017

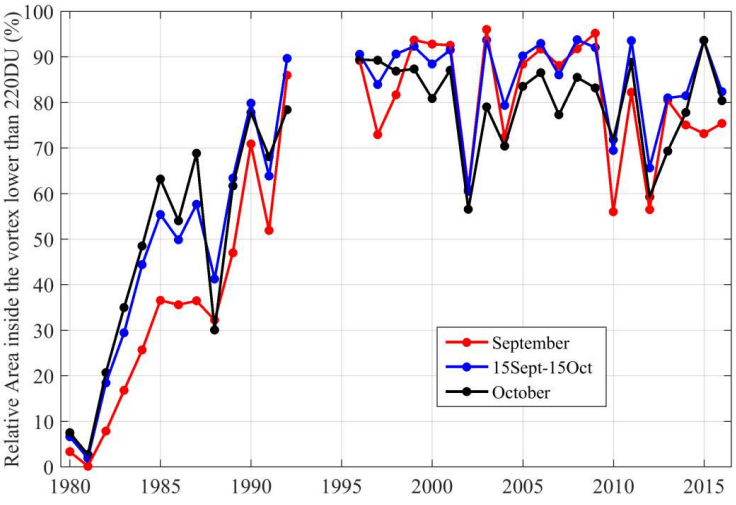

Figure 12: Relative area inside the vortex (in %) lower than 220 DU computed from TOMS/OMIT dataset using 400K-600K classification on September, 15Sept-15Oct and October.